IEEE Access
Multidisciplinary | Rapid Review | Open Access Journal

Received August 27, 2019, accepted September 21, 2019, date of publication October 8, 2019, date of current version October 24, 2019.

Digital Object Identifier 10.1109/ACCESS.2019.2946339

Circular θ-QAM: A Circle-Shaped QAM for Higher-Order Modulation

SEONGJIN AHN, (Student Member, IEEE), AND DONGWEON YOON, (Senior Member, IEEE)
Department of Electronics and Computer Engineering, Hanyang University, Seoul 04763, Korea

Corresponding author: Dongweon Yoon (dwyoon@hanyang.ac.kr)

This work was supported by the Institute of Information and Communications Technology Planning and Evaluation (IITP) Grant funded by the Korean Government (MSIT) (No. 2017-0-01703, Wireless Transmission System for Full-Parallax Multiview).

ABSTRACT This paper proposes M-ary circular θ-quadrature amplitude modulation (CTQAM) for $M = 2^l$, $l \geq 4$, which is constructed by rearrangement of the signal points based on θ-QAM. We provide a construction method for the signal constellation of CTQAM and analyze the symbol and bit error performances of M-ary CTQAM in additive white Gaussian noise (AWGN) and Nakagami-m fading channels. Through computer simulations, we validate theoretical results.

INDEX TERMS Quadrature amplitude modulation, higher-order modulation, error probability.

I. INTRODUCTION

In contemporary communication and broadcasting systems, higher-order modulation is required for high speed data transmission. Since quadrature amplitude modulation (QAM) can achieve high data rate transmission without additional bandwidth, it has been widely studied as a method for higher-order modulation. In particular, a considerable amount of research on square QAM (SQAM) has been conducted [1]–[3], and SQAM has been adopted in many practical systems due to the simplicity of modulation and demodulation methods [4]–[6]. Although SQAM offers low complexity of modulation and demodulation methods, it does not provide optimal error performance. To minimize the error probability of QAM, Foschini *et al.*, using an asymptotic (large signal-to-noise ratio) expression, suggested a modified gradient-search procedure that converges to an optimal constellation [7]. In [7], it was shown that the optimal constellation forms a lattice of equilateral triangles and takes on a circle shape as the number of signal points increases, which provides the minimum average symbol energy for a given minimum Euclidean distance. Although the optimal constellation in [7] provides the minimum error probability, it is not suitable for practical applications due to the presence of signal points at the origin and axis, and irregular decision regions.

To overcome these hindrances of the optimal constellation, more practical constellations were proposed without signal points at the origin and axis, and having symmetric decision regions about the origin. Triangular QAM (TQAM), and θ-QAM including SQAM and TQAM as special cases, were proposed in [8] and [9], respectively, which have better error performance than SQAM. Recently, stepped θ-QAM based on θ-QAM was proposed in [10], which provides better error performance than θ-QAM. Stepped θ-QAM, however, does not form a circle shape as the number of signal points increases. Therefore, there is room for improvement of the error performance and peak-to-average power ratio (PAPR): if we can make θ-QAM into a circle shape, the average symbol energy for a given minimum Euclidean distance, and PAPR can be reduced.

In this paper, we propose a circle-shaped quadrature amplitude modulation for higher-order modulation, M-ary circular θ-QAM (CTQAM), for $M = 2^l$, $l \geq 4$ based on θ-QAM, which minimizes the average symbol energy for a given minimum Euclidean distance, among all the constellations with θ-QAM lattice. The construction method for the signal constellation of CTQAM is provided, and it is shown that the average symbol energy and PAPR of CTQAM for a given M, are less than those of stepped θ-QAM. Then, we analyze the symbol and bit error performances in additive white Gaussian noise (AWGN) and Nakagami-m fading channels. Finally, we validate theoretical error performance results through computer simulations.

II. CIRCULAR θ-QAM

A. SIGNAL CONSTELLATIONS

M-ary CTQAM for $M = 2^l$, $l \geq 4$ is constructed by an iterative rearrangement process of the signal points of M-ary θ-QAM.

The associate editor coordinating the review of this manuscript and approving it for publication was Maurizio Magarini.

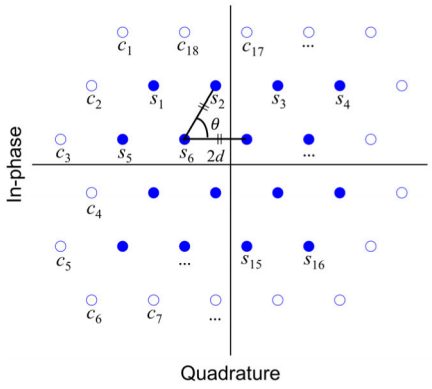

FIGURE 1. Signal points of 16-ary θ-QAM ($\theta = 60°$) and candidate signal points.

Let $\mathbf{S} = \{s_1, \cdots, s_M\}$ be the set of the signal points and $\mathbf{C} = \{c_1, \cdots, c_N | \mathbf{S}\}$ be the set of the candidate signal points given $\mathbf{S}$. For this case, the initial set $\mathbf{S}$ is equal to the set of the signal points of M-ary θ-QAM, $\mathbf{S}_{M-\text{ary}\theta-\text{QAM}}$, and each signal point is represented by $s_1, \cdots, s_M$ from left to right, top to bottom. Subsequently, under the condition of maintaining the lattice of M-ary θ-QAM, the vacant locations adjacent to the top, bottom, left and right signal points on the edge are set as the candidate signal points, and each candidate signal point is represented by $c_1, \cdots, c_N$ in the counterclockwise direction from the top left. As an example, we depict the signal points of 16-ary θ-QAM ($\theta = 60°$) and candidate signal points in Fig. 1, where $2d$ is the minimum Euclidean distance between two adjacent signal points. If we denote an arbitrary signal point s_k and an arbitrary candidate signal point c_h by coordinate pairs $(s_{k,I}, s_{k,Q})$ and $(c_{h,I}, c_{h,Q})$, the magnitudes of s_k and c_h can be computed as

$$\|s_k\| = \sqrt{s_{k,I}^2 + s_{k,Q}^2} \tag{1}$$

$$\|c_h\| = \sqrt{c_{h,I}^2 + c_{h,Q}^2} \tag{2}$$

where $k = 1, 2, \cdots, M$; $h = 1, 2, \cdots, N$; $s_{k,I}$ and $s_{k,Q}$ are the in-phase and quadrature values of s_k; and $c_{h,I}$ and $c_{h,Q}$ are the in-phase and quadrature values of c_h. Let $s_{\max}$ be the signal point with the maximum magnitude in $\mathbf{S}$ and $c_{\min}$ be the candidate signal point with the minimum magnitude in $\mathbf{C}$. Then, the rearrangement of the signal points of M-ary θ-QAM to construct M-ary CTQAM is performed by comparing $s_{\max}$ and $c_{\min}$. The detailed construction method of M-ary CTQAM is as follows.

First, as mentioned above, the initial values of $\mathbf{S}$ and $\mathbf{C}$ are determined based on M-ary θ-QAM. If the magnitude of $s_{\max}$ is greater than that of $c_{\min}$, $s_{\max}$ is excluded from the signal point and $c_{\min}$ is included in a new signal point to generate a new set of signal points $\mathbf{S}$. Then, a new set of candidate signal points $\mathbf{C}$ is generated based on the new set of the signal points $\mathbf{S}$. Rearrangement is repeated by using newly generated $\mathbf{S}$ and $\mathbf{C}$ until the magnitude of every $s_{\max}$ is less than or equal to that of $c_{\min}$.

Following the steps above, we formulate the construction method of M-ary CTQAM in pseudo code as follows:

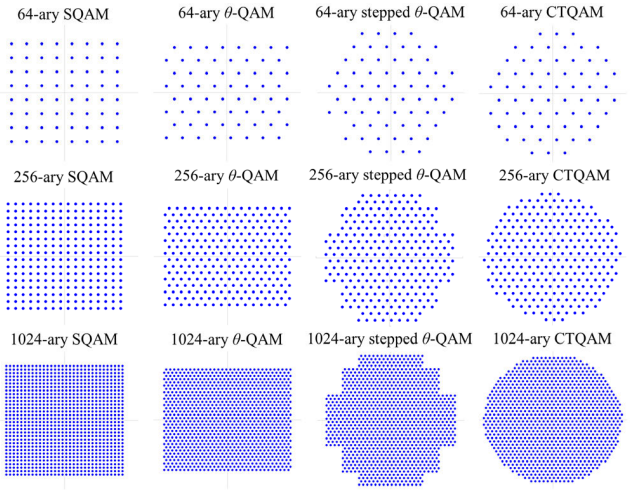

FIGURE 2. Signal constellations of 64–, 256–, and, 1024-ary SQAM, θ-QAM, stepped θ-QAM, and CTQAM for $\theta = 60°$.

Algorithm 1 Construction Method of M-ary CTQAM

Initialization:
$\mathbf{S} = \{s_1, \cdots, s_M\}$; $s_k \in \mathbf{S}_{M-\text{ary}\,\theta-\text{QAM}}$, $k = 1, \cdots, M$;
$\mathbf{C} = \{c_1, \cdots, c_N | \mathbf{S}\}$;
while $\max_{s_k \in S} \|s_k\| > \min_{c_h \in C} \|c_h\|$; $k = 1, \cdots, M$, $h = 1, \cdots, N$
$s_{\max} = \arg\max_{s_k \in S} \|s_k\|$;
$c_{\min} = \arg\min_{c_h \in C} \|c_h\|$;
$\mathbf{S} = \mathbf{S} - \{s_{\max}\} + \{c_{\min}\}$;
$\mathbf{C} = \{c_1, \cdots, c_{N_{\text{new}}} | \mathbf{S}\}$;
$N = N_{\text{new}}$;
end

Fig. 2 shows the signal constellations of CTQAM obtained from the above construction method and conventional QAMs, e.g., SQAM, θ-QAM, and stepped θ-QAM, for various M when $\theta = 60°$. Fig. 3 depicts the signal constellations of 256-ary CTQAM for various values of θ. Note in Fig. 2 that CTQAM has a circular shape compared with the conventional QAMs and becomes more circular as the modulation order M increases.

B. AVERAGE SYMBOL ENERGY AND PEAK-TO-AVERAGE POWER RATIO

The average symbol energy E_{avg} and PAPR can be calculated by

$$E_{\text{avg}} = \frac{1}{M} \sum_{k=1}^{M} \left(s_{k,I}^2 + s_{k,Q}^2 \right) \tag{3}$$

$$\text{PAPR} = \frac{P_{\text{peak}}}{P_{\text{avg}}} = \frac{\max_{k \in [1,M]} \left(s_{k,I}^2 + s_{k,Q}^2 \right)}{\frac{1}{M} \sum_{k=1}^{M} \left(s_{k,I}^2 + s_{k,Q}^2 \right)} \tag{4}$$

TABLE 1. Comparisons of the average symbol energy and PAPR.

M	SQAM		θ-QAM		Stepped θ-QAM		CTQAM	
	E_{avg}	PAPR	E_{avg}	PAPR	E_{avg}	PAPR	E_{avg}	PAPR
64	$42d^2$	2.3333	$37d^2$	2.5135	$35.6d^2$	2.0491	$35.3d^2$	1.9007
256	$170d^2$	2.6471	$149d^2$	2.7450	$143.5d^2$	2.2787	$141.2d^2$	1.9757
1024	$682d^2$	2.8182	$597d^2$	2.8693	$575d^2$	2.4017	$564.6d^2$	1.9958
4096	$2730d^2$	2.9077	$2389d^2$	2.9339	$2301d^2$	2.4654	$2258.2d^2$	2.0139

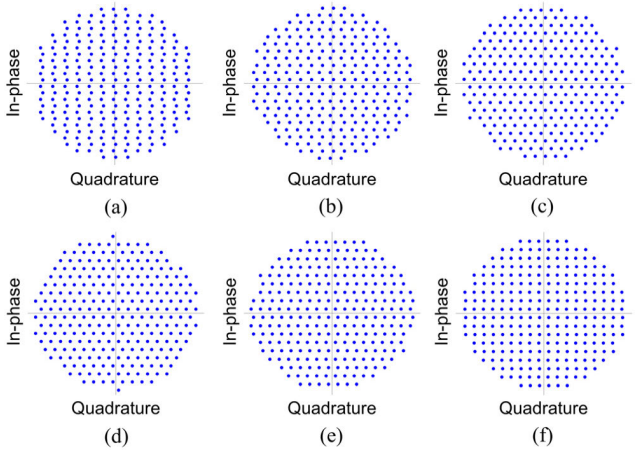

FIGURE 3. Signal constellations of 256-ary CTQAM for various values of θ. (a) $\theta = 35°$. (b) $\theta = 45°$. (c) $\theta = 55°$. (d) $\theta = 65°$. (e) $\theta = 75°$. (f) $\theta = 85°$.

where P_{avg} and P_{peak} denote the average power and peak power, respectively. We can expect both the average symbol energy and PAPR for a given minimum Euclidean distance to be reduced, because in the proposed construction method a signal point of greater magnitude is rearranged to a new signal point of smaller magnitude, which leads the signal constellation of M-ary CTQAM to become circular as M increases.

We tabulate E_{avg} and PAPR of SQAM, θ-QAM, stepped θ-QAM, and CTQAM in Table 1, where we assume a minimum Euclidean distance of $2d$ and $\theta = 60°$. As shown in Table 1, CTQAM has lower average symbol energy and lower PAPR than SQAM, θ-QAM, and stepped θ-QAM, and the differences of the average symbol energy and of the PAPR between CTQAM and other modulation schemes become larger as the modulation order M increases. We therefore expect CTQAM to show better error performance than other modulation schemes and the error performance difference to increase as the modulation order increases.

C. BIT-TO-SYMBOL MAPPING

For higher-order modulation, it is important to find optimal bit-to-symbol mapping based on minimizing the bit errors for a given symbol error. In general, since it is likely that most symbol errors occur between adjacent symbols, optimal bit-to-symbol mapping can be obtained by finding a

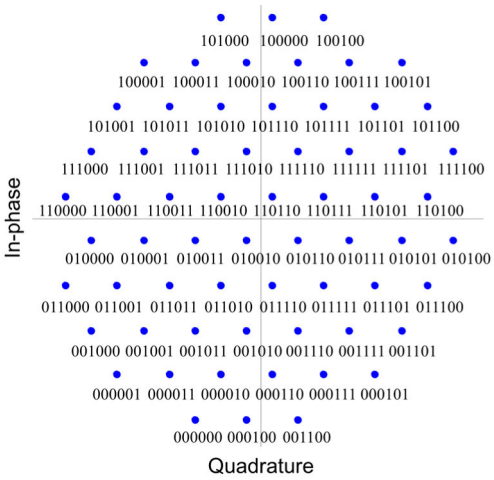

FIGURE 4. Bit-to-symbol mapping of 64-ary CTQAM.

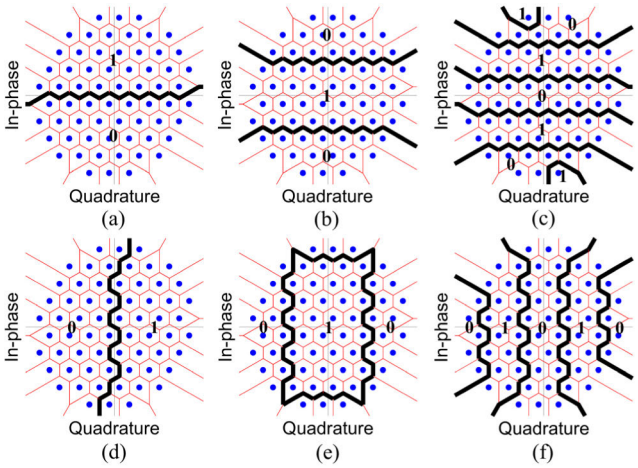

FIGURE 5. Decision regions for the (a) first bit, (b) second bit, (c) third bit, (d) fourth bit, (e) fifth bit, and (f) sixth bit of 64-ary CTQAM.

bit-to-symbol mapping that has the minimum average Hamming distance. Theoretically, optimal bit-to-symbol mapping of the signal constellation with the modulation order M can be found by performing all possible searches, which would involve $M!$ possible candidates. This becomes impracticable as M increases. Therefore, we adopt a suboptimal bit-to-symbol mapping scheme, the layer labeling algorithm proposed in [11] that is applicable to high modulation orders without prohibitively huge searches. In this paper we assume that the search limit N_e, which is the key parameter of the layer labeling algorithm, is 9 as in [11].

Fig. 4 shows a bit-to-symbol mapping of 64-ary CTQAM, as an example, by using the layer labeling algorithm. The decision regions for each bit of 64-ary CTQAM are depicted in Fig. 5. Note that the decision regions in Fig. 5 are all symmetrical about the origin. Similarly, for a higher modulation order M, we can also obtain bit-to-symbol mapping and the decision regions for each bit, showing symmetry about the origin.

III. EXACT ERROR PROBABILITY OF CIRCULAR θ-QAM

In this section, we analyze the exact symbol error rate (SER) and bit error rate (BER) of M-ary CTQAM, where the exact SER and BER expressions are provided in terms of a two-dimensional (2-D) Gaussian Q-function [12].

The exact SER in an AWGN channel, P_{SER}, can be presented in terms of the error probabilities of the closed decision region (R^c), P^c_{SER}, and the open decision region (R^o), P^o_{SER}, [13]

$$\begin{aligned} P_{\text{SER}} &= P^c_{\text{SER}} + P^o_{\text{SER}} \\ &= \sum_{k=1}^{U} \left[\left(1 - P\left\{s_r \in R^c_k | s_t = s^c_k\right\}\right) P\left\{s^c_k\right\} \right] \\ &\quad + \sum_{k=1}^{V} \left[\left(1 - P\left\{s_r \in R^o_k | s_t = s^o_k\right\}\right) P\left\{s^o_k\right\} \right] \end{aligned} \tag{5}$$

where U and V are the numbers of the closed and open decision regions; s^c and s^o are the signal points with the closed and open decision regions, respectively; s_r and s_t are the received and transmitted signals; R_k is the decision region of the signal point s_k; and $P\{s_k\}$ is the *a priori* probability. Note that in (5), the conditional probability $P\{s_r \in R_k | s_t = s_k\}$ that the received signal s_r falls into the decision region R_k, given that the transmitted signal s_t is s_k, can be obtained by using the 2-D Gaussian Q-function [13].

For the closed decision regions, the conditional probability can be obtained as

$$\begin{aligned} &P\left\{s_r \in R^c_k | s_t = s^c_k\right\} \\ &= Q\left(\frac{E[Y_1]}{\sqrt{\text{Var}[Y_1]}}, \frac{E[Y_2]}{\sqrt{\text{Var}[Y_2]}}; \rho_{Y_1Y_2}\right) \\ &\quad + Q\left(-\frac{E[Y_1]}{\sqrt{\text{Var}[Y_1]}}, -\frac{E[Y_n]}{\sqrt{\text{Var}[Y_n]}}; \rho_{Y_1Y_n}\right) \\ &\quad - \sum_{k=2}^{n-1} Q\left(\frac{E[Y_k]}{\sqrt{\text{Var}[Y_k]}}, -\frac{E[Y_{k+1}]}{\sqrt{\text{Var}[Y_{k+1}]}}; -\rho_{Y_kY_{k+1}}\right) \end{aligned} \tag{6}$$

and for the open decision regions, it can be expressed as

$$\begin{aligned} &P\left\{s_r \in R^o_k | s_t = s^o_k\right\} \\ &= Q\left(\frac{E[Y_1]}{\sqrt{\text{Var}[Y_1]}}, \frac{E[Y_2]}{\sqrt{\text{Var}[Y_2]}}; \rho_{Y_1Y_2}\right) \\ &\quad - \sum_{k=2}^{q-1} Q\left(\frac{E[Y_k]}{\sqrt{\text{Var}[Y_k]}}, -\frac{E[Y_{k+1}]}{\sqrt{\text{Var}[Y_{k+1}]}}; -\rho_{Y_kY_{k+1}}\right) \end{aligned} \tag{7}$$

where n and q are the numbers of sides of the polygonal closed and open decision regions; $E[Y_k] = s_{k,\,Q}\cos\varphi_k - s_{k,\,I}\cdot\sin\varphi_k - d_k$ is the expectation of Y_k which is a vertical line to the kth decision boundary X_k of the decision region; φ_k is the rotation angle between the in-phase axis and X_k; $\text{Var}[Y_k] = \sigma^2$ is the variance of Y_k; and d_k is the distance from the origin to X_k [13].

We depict the decision regions for the signal points of 64-ary CTQAM in Fig. 6 to obtain the exact SER of 64-ary CTQAM, when $\theta = 60°$, as an example. There are four different types of decision regions D_i, $i = 1, 2, 3, 4$, and the conditional probabilities for each decision region, P_{D_i}, can be calculated by

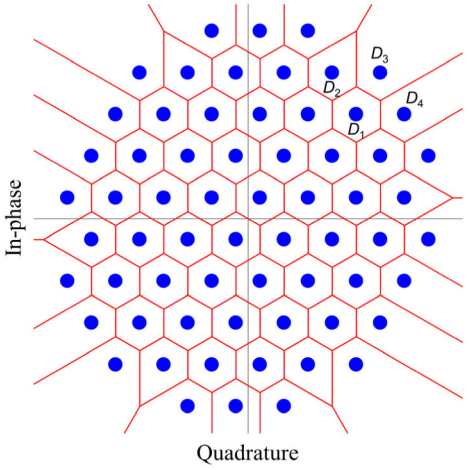

FIGURE 6. Decision regions for the signal points of 64-ary CTQAM.

$$\begin{aligned} P_{D_1} &= Q\left(-\sqrt{\frac{8E_b}{47N_0}}, -\sqrt{\frac{8E_b}{47N_0}}, \frac{1}{2}\right) \\ &\quad + Q\left(\sqrt{\frac{8E_b}{47N_0}}, \sqrt{\frac{8E_b}{47N_0}}, \frac{1}{2}\right) \\ &\quad - 4Q\left(-\sqrt{\frac{8E_b}{47N_0}}, \sqrt{\frac{8E_b}{47N_0}}, -\frac{1}{2}\right) \\ P_{D_2} &= Q\left(-\sqrt{\frac{8E_b}{47N_0}}, -\sqrt{\frac{8E_b}{47N_0}}, \frac{1}{2}\right) \\ &\quad + Q\left(\sqrt{\frac{8E_b}{47N_0}}, \sqrt{\frac{8E_b}{47N_0}}, -\frac{1}{2}\right) \\ &\quad - 3Q\left(-\sqrt{\frac{8E_b}{47N_0}}, \sqrt{\frac{8E_b}{47N_0}}, -\frac{1}{2}\right) \\ P_{D_3} &= Q\left(-\sqrt{\frac{8E_b}{47N_0}}, -\sqrt{\frac{8E_b}{47N_0}}, \frac{1}{2}\right) \\ &\quad - Q\left(-\sqrt{\frac{8E_b}{47N_0}}, \sqrt{\frac{8E_b}{47N_0}}, -\frac{1}{2}\right) \\ &\quad - Q\left(-\sqrt{\frac{8E_b}{47N_0}}, \sqrt{\frac{24E_b}{47N_0}}, -\frac{\sqrt{3}}{2}\right) \\ P_{D_4} &= Q\left(-\sqrt{\frac{8E_b}{47N_0}}, -\sqrt{\frac{8E_b}{47N_0}}, \frac{1}{2}\right) \\ &\quad - 2Q\left(-\sqrt{\frac{8E_b}{47N_0}}, \sqrt{\frac{8E_b}{47N_0}}, -\frac{1}{2}\right) \end{aligned} \tag{8}$$

where E_b / N_0 denotes the bit energy-to-noise spectral density ratio. The numbers of each type of decision region N_{D_i}, $i = 1, 2, 3, 4$, are $N_{D_1} = 38$, $N_{D_2} = 6$, $N_{D_3} = 12$,

and $N_{D_4} = 8$. If we assume that the symbols are equally likely to be transmitted, then the exact SER of 64-ary CTQAM for $\theta = 60°$ is obtained as

$$\begin{aligned} P_{\text{SER, 64}} &= 1 - Q\left(-\sqrt{\frac{8E_b}{47N_0}}, -\sqrt{\frac{8E_b}{47N_0}}, \frac{1}{2}\right) \\ &\quad - \frac{19}{32}Q\left(\sqrt{\frac{8E_b}{47N_0}}, \sqrt{\frac{8E_b}{47N_0}}, \frac{1}{2}\right) \\ &\quad + \frac{99}{32}Q\left(-\sqrt{\frac{8E_b}{47N_0}}, \sqrt{\frac{8E_b}{47N_0}}, -\frac{1}{2}\right) \\ &\quad - \frac{3}{32}Q\left(\sqrt{\frac{8E_b}{47N_0}}, \sqrt{\frac{8E_b}{47N_0}}, -\frac{1}{2}\right) \\ &\quad + \frac{3}{16}Q\left(-\sqrt{\frac{8E_b}{47N_0}}, \sqrt{\frac{24E_b}{47N_0}}, -\frac{\sqrt{3}}{2}\right). \end{aligned} \tag{9}$$

Similarly, for other values of M and θ, the exact SER of M-ary CTQAM can also be obtained by the 2-D Gaussian Q-function.

Meanwhile, the exact BER in an AWGN channel has the form of [14]

$$P_{BER} = \frac{1}{\log_2 M}\sum_{h=1}^{M}\sum_{k=1,\,k\neq h}^{M} H(v_h,\ v_k) \times P\{s_r \in R_k | s_t = s_h\}P\{s_h\} \tag{10}$$

where v_h, $h = 1, \cdots, M$, denotes the bit pattern assigned to the signal point s_h, and $H(v_h, v_k)$ is the Hamming distance between v_h and v_k.

In a fading channel, the instantaneous signal-to-noise power ratio (SNR) per bit, γ, of the received signal will be a random variable, whose probability density function (pdf), $f_\gamma(\gamma)$, is dependent on the nature of the fading channel [15]. Then, the exact SER in the fading channel, $P_{\text{SER\_}f}$, is evaluated by averaging (5) over $f_\gamma(\gamma)$, which can be generalized as (11) after manipulations of [12, (26.3.8) and (26.3.9)] [16],

$$\begin{aligned} &P_{\text{SER\_}f} \\ &= \int_0^\infty P_{\text{SER}} f_\gamma(\gamma)d\gamma \\ &= \frac{1}{M}\left[\sum_{h=1}^{U}\left[\sum_{i=1}^{n}\left\{\Psi_{1-D}\left(z_i\sqrt{\gamma}\right)\right.\right.\right. \\ &\quad \left.\left.\left. - \ \Psi_{2-D}\left(z_i\sqrt{\gamma}, z_{i+1}\sqrt{\gamma}\right)\right\}\right]_{s_t=s_h^c} \\ &\quad + \sum_{k=1}^{V}\left[\sum_{i=1}^{q}\Psi_{1-D}\left(z_i\sqrt{\gamma}\right)\right. \\ &\quad \left. - \sum_{i=1}^{q-1}\Psi_{2-D}\left(z_i\sqrt{\gamma}, z_{i+1}\sqrt{\gamma}\right)\right]_{s_t=s_k^o} \end{aligned} \tag{11}$$

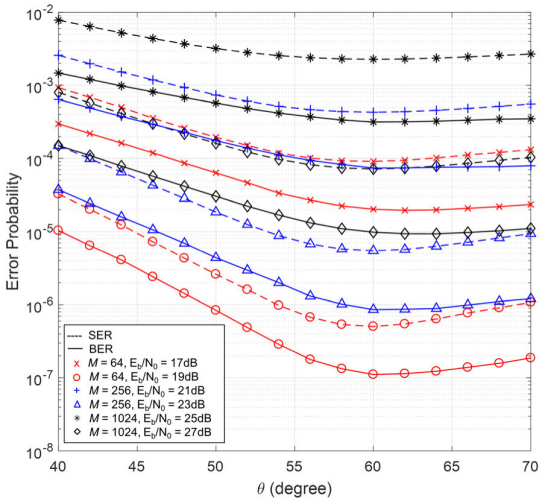

FIGURE 7. SER and BER of M -ary CTQAM versus θ in an AWGN channel.

where

$$\begin{aligned} \Psi_{1-D}\left(z_i\sqrt{\gamma}\right) &= \int_0^\infty Q\left(z_i\sqrt{\gamma}\right)f_\gamma(\gamma)d\gamma; \\ \Psi_{2-D}\left(z_i\sqrt{\gamma}, z_{i+1}\sqrt{\gamma}\right) &= \int_0^\infty Q\left(z_i\sqrt{\gamma}, z_{i+1}\sqrt{\gamma}; \rho_{Y_iY_{i+1}}\right) \\ &\quad \times f_\gamma(\gamma)d\gamma; \end{aligned}$$

and $z_i = -E[Y_i]/\sqrt{\gamma Var[Y_i]}$.

In the case of Nakagami-m fading channel, as an example, the pdf of γ becomes the Gamma distribution [15]

$$f_\gamma(\gamma) = \frac{m^m\gamma^{m-1}}{\bar{\gamma}^m\Gamma(m)}\exp\left(-\frac{m\gamma}{\bar{\gamma}}\right), \quad \gamma \geq 0 \tag{12}$$

where $\bar{\gamma}$ is the average SNR per bit and $\Gamma(\cdot)$ denotes the Gamma function [12]. Then, $\Psi_{1-D}\left(z_i\sqrt{\gamma}\right)$ and $\Psi_{2-D}\left(z_i\sqrt{\gamma}, z_{i+1}\sqrt{\gamma}\right)$ can be obtained as closed-form solutions [16],

$$\begin{aligned} &\Psi_{1-D}\left(z_i\sqrt{\gamma}\right) \\ &= \frac{1}{2} - \frac{1}{2}\sqrt{\frac{z_i^2\bar{\gamma}}{2m + z_i^2\bar{\gamma}}}\sum_{k=0}^{m-1}{}_{2k}C_k\left[\frac{\left(1 - \frac{z_i^2\bar{\gamma}}{2m+z_i^2\bar{\gamma}}\right)}{4}\right]^k \end{aligned} \tag{13}$$

$$\begin{aligned} &\Psi_{2-D}\left(z_i\sqrt{\gamma}, z_{i+1}\sqrt{\gamma}\right) \\ &= \frac{1}{2}\sum_{k=i}^{i+1}\left[\frac{\omega_k}{\pi} - \frac{1}{\pi}\beta\left[\left(\frac{\pi}{2} + \tan^{-1}\alpha\right)\Omega_1\right.\right. \\ &\quad \left.\left. + \ \sin\left(\tan^{-1}\alpha\right)\Omega_2\right]\right] \end{aligned} \tag{14}$$

where

$$\begin{aligned} \alpha &= -\beta\cot\omega_k, \quad \beta = \sqrt{\frac{c}{1+c}}\text{sgn}\omega_k \\ c &= \frac{z_i^2\bar{\gamma}}{2m}, \quad \Omega_1 = \sum_{h=0}^{m-1}\frac{{}_{2h}C_h}{(4(1+c))^h}, \\ \Omega_2 &= \sum_{h=1}^{m-1}\sum_{i=1}^{h}\frac{{}_{2h}C_h}{2(h-i)C_{h-i}(2(h-i)+1)4^i(1+c)} \\ &\quad \times \cos^{2(h-i)+1}(\tan^{-1}\alpha). \end{aligned} \tag{15}$$

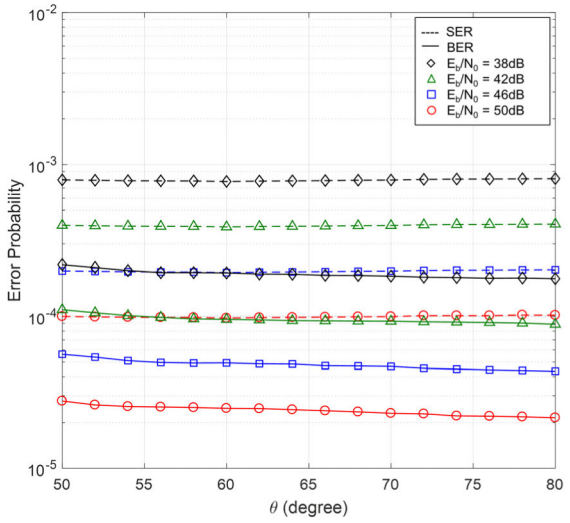

(a)

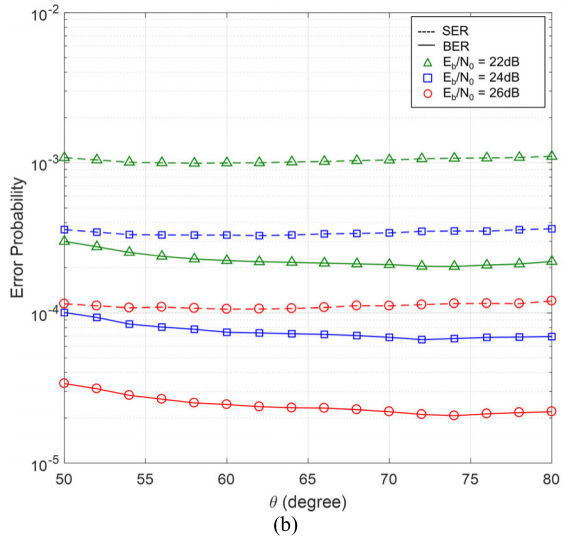

(b)

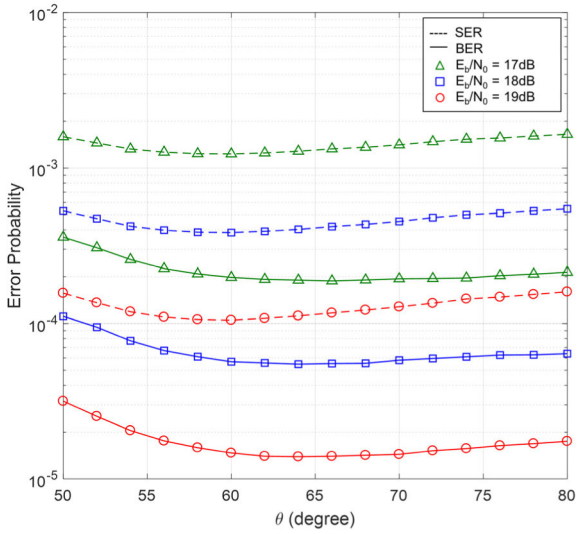

(c)

FIGURE 8. SER and BER of 64-ary CTQAM versus θ in Nakagami-m fading channels. (a) $m = 1$. (b) $m = 2.5$. (c) $m = 10$.

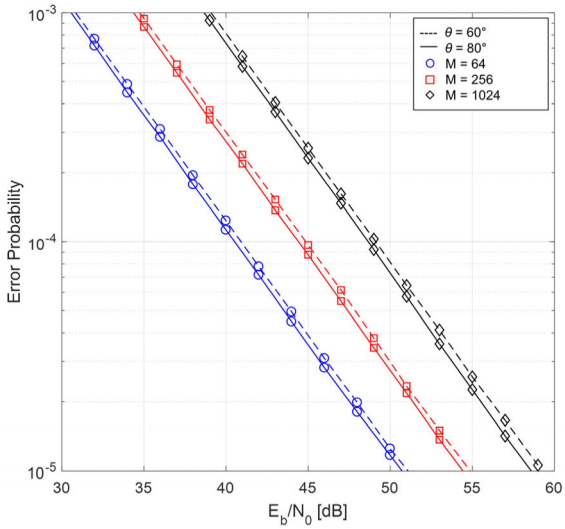

FIGURE 9. BER of 64−, 256−, and 1024-ary CTQAM for $\theta = 60°$ and 80° in Nakagami-m fading channel when $m = 1$.

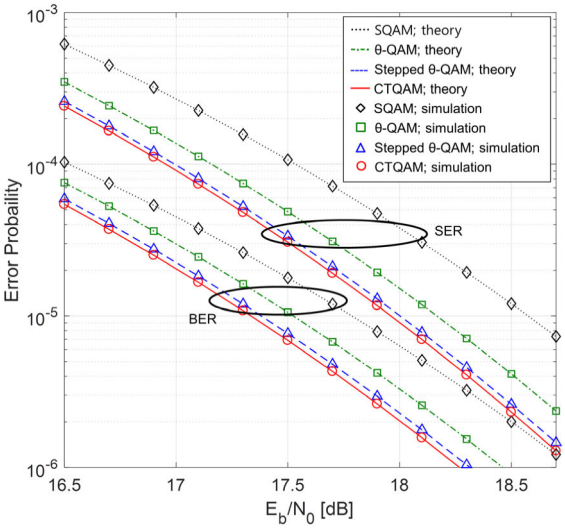

FIGURE 10. SER and BER of 64-ary SQAM, θ-QAM, stepped θ-QAM, and CTQAM in an AWGN channel.

By substituting (13) and (14) into (11), we can obtain the exact SER in Nakagami-m fading channels. Analogously, the exact BER in Nakagami-m fading channels can be obtained by averaging (10) over (12).

IV. NUMERICAL RESULTS

In this section, we validate the theoretical SER and BER results of CTQAM in AWGN and Nakagami-m fading channels by computer simulations. We include the results of conventional QAMs, e.g., SQAM, θ-QAM, and stepped θ-QAM for comparison.

Fig. 7 shows the SER and BER versus θ of M-ary CTQAM in an AWGN channel for specific E_b/N_0 values. Note in Fig. 7 that the optimal angles in terms of minimum SER and BER are $\theta \approx 60°$ regardless of M, as shown in [9] and [13].

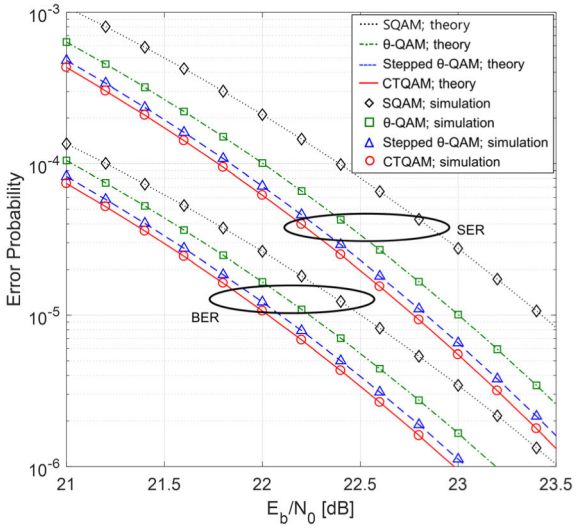

FIGURE 11. SER and BER of 256-ary SQAM, θ-QAM, stepped θ-QAM, and CTQAM in an AWGN channel.

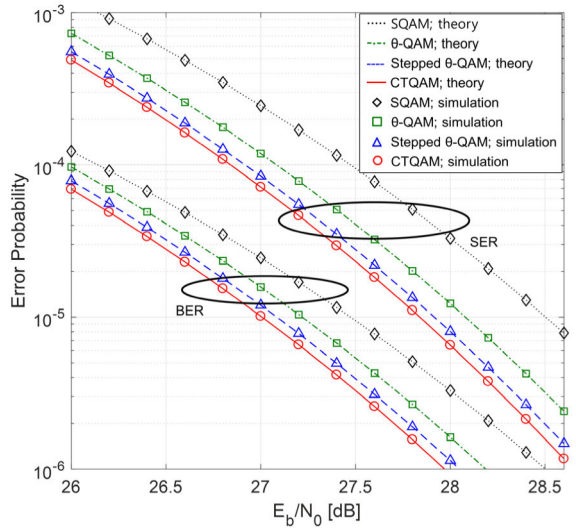

FIGURE 12. SER and BER of 1024-ary SQAM, θ-QAM, stepped θ-QAM, and CTQAM in an AWGN channel.

Fig. 8 shows the SER and BER of 64-ary CTQAM versus θ in Nakagami-m fading channels for specific E_b/N_0 values when $m = 1, 2.5$, and 10. We see in Fig. 8 that the optimal angles in terms of minimum SER are $\theta \approx 60°$ regardless of the fading severity m, but the angles in terms of BER vary with m. Concerning BER, when $m = 1$, which results in Rayleigh fading channel, the optimal angle is $\theta \approx 80°$. When $m = 2.5$ and 10, the optimal angles are $\theta \approx 75°$ and 65°, respectively, and as the fading severity m approaches infinity, where $m = \infty$ corresponds to an AWGN channel, the optimal angle converges to $\theta = 60°$, as seen in Fig. 7. For other modulation orders, we have observed a similar tendency, as in $M = 64$ where the optimal angles in terms of BER vary with the fading severity m.

Fig. 9 depicts the BER of 64−, 256−, and 1024-ary CTQAM for $\theta = 60°$ and 80° in Nakagami-m fading channel

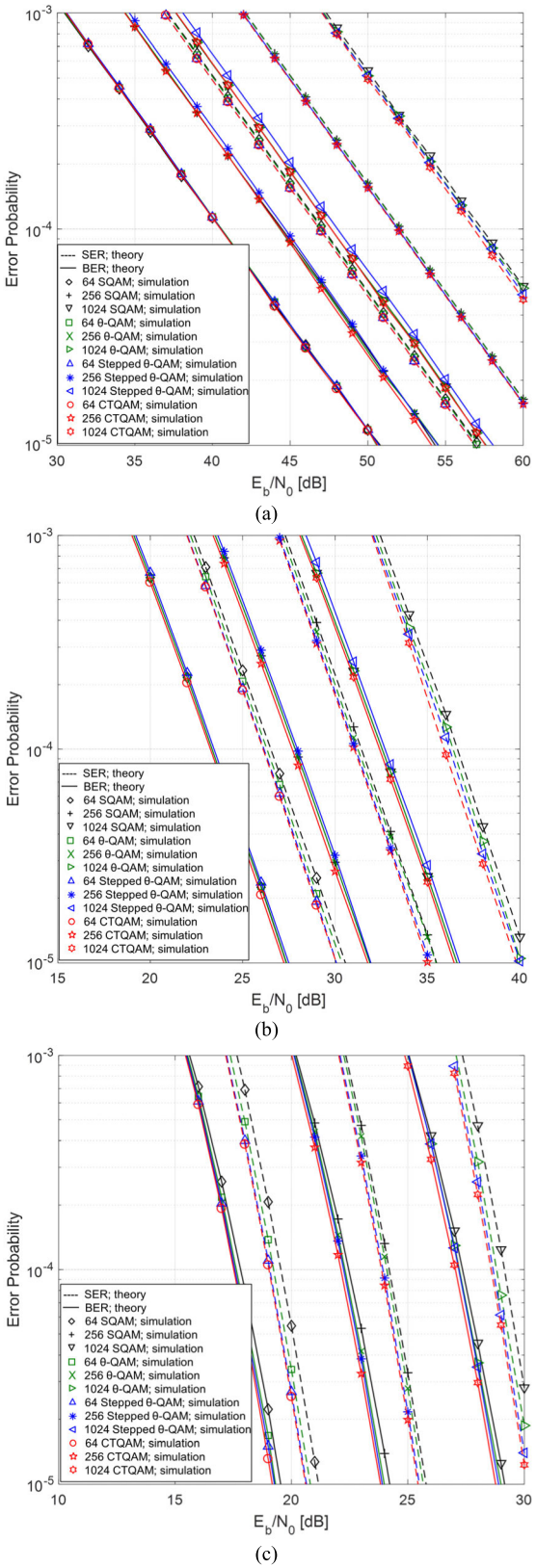

FIGURE 13. SER and BER of 64−, 256− and 1024-ary SQAM, θ-QAM, stepped θ-QAM, and CTQAM in Nakagami-m fading channels. (a) $m = 1$. (b) $m = 2.5$. (c) $m = 10$.

when $m = 1$, and we see that the BERs for $\theta = 60°$ and for $\theta = 80°$ differ by about 10%.

Fig. 10 shows the SER and BER versus E_b/N_0 of 64-ary SQAM, θ-QAM, stepped θ-QAM, and CTQAM in an AWGN channel, when $\theta = 60°$. As shown in Fig. 10, 64-ary CTQAM achieves power gains of about 0.6 dB, 0.2 dB, and 0.05 dB at the SER of 10^{-5}, and 0.46 dB, 0.18 dB, and 0.04 dB at the BER of 10^{-5} over 64-ary SQAM, θ-QAM, and stepped θ-QAM, respectively. CTQAM outperforms other modulation schemes in the error rates because CTQAM has lower average symbol energy for a given minimum Euclidean distance, as shown in Table 1.

We also depict the SER and BER of 256- and 1024-ary SQAM, θ-QAM, stepped θ-QAM, and CTQAM in an AWGN channel, when $\theta = 60°$, in Figs. 11 and 12, respectively. From Figs. 10, 11, and 12, we find that power gains of CTQAM over the conventional QAMs get larger as the modulation order M increases.

Fig. 13 shows the SER and BER versus E_b/N_0 of 64-, 256- and 1024-ary SQAM, θ-QAM, stepped θ-QAM, and CTQAM in Nakagami-m fading channels when $m = 1, 2.5$, and 10, where the optimal angles for each constellation are considered. In Fig. 13, we can see that CTQAM shows better error performance than the conventional QAMs, except when $m = 1$, in which case all QAM schemes show almost the same error performance. Note in Table 1 that CTQAM has lower PAPR than the conventional QAMs and hence CTQAM can be a good choice even in Nakagami-m fading channels.

V. CONCLUSION

In this paper, we proposed M-ary CTQAM for $M = 2^l$, $l \geq 4$, which is constructed by rearrangement of the signal points based on θ-QAM. We presented the construction method for the signal constellation of CTQAM and showed that the average symbol energy and PAPR of CTQAM are lower than those of conventional QAMs, e.g., SQAM, θ-QAM, and stepped θ-QAM, for a given minimum Euclidean distance. We then provided the SER and BER performances in AWGN and Nakagami-m fading channels, where the proposed CTQAM offers better error performance than the conventional QAMs. The proposed CTQAM could enable future communication and broadcasting systems to transmit large amounts of data with higher power efficiency and reliability.

REFERENCES

[1] C. N. Campopiano and B. G. Glazer, "A coherent digital amplitude and phase modulation scheme," *IRE Trans. Commun. Syst.*, vol. 10, no. 1, pp. 90–95, Mar. 1962.

[2] W. Webb and L. Hanzo, *Modern Quadrature Amplitude Modulation: Principles and Applications for Fixed and Wireless Communications*. New York, NY, USA: IEEE Press, 1994.

[3] K. Cho and D. Yoon, "On the general BER expression of one- and two-dimensional amplitude modulations," *IEEE Trans. Commun.*, vol. 50, no. 7, pp. 1074–1080, Jul. 2002.

[4] *Digital Video Broadcasting (DVB); Framing Structure Channel Coding and Modulation for a Second Generation Digital Terrestrial Television Broadcasting System (DVB-T2)*, document ETSI EN 302 755 v.1.4.1, Jul. 2015.

[5] *IEEE Standard for Information Technology–Telecommunications and Information Exchange Between Systems Local and Metropolitan Area Networks–Specific Requirements—Part 11: Wireless LAN Medium Access Control (MAC) and Physical Layer (PHY) Specifications*, IEEE Standard 802.11-2016, 2016.

[6] *LTE; Evolved Universal Terrestrial Radio Access (E-UTRA); Physical Channels and Modulation*, document ETSI TS 136 211 v.14.2.0, Jan. 2018.

[7] G. Foschini, R. Gitlin, and S. Weinstein, "Optimization of two-dimensional signal constellations in the presence of Gaussian noise," *IEEE Trans. Commun.*, vol. 22, no. 1, pp. 28–38, Jan. 1974.

[8] S. J. Park, "Triangular quadrature amplitude modulation," *IEEE Commun. Lett.*, vol. 11, no. 4, pp. 292–294, Apr. 2007.

[9] K. N. Pappi, A. S. Lioumpas, and G. K. Karagiannidis, "θ-QAM: A parametric quadrature amplitude modulation family and its performance in AWGN and fading channels," *IEEE Trans. Commun.*, vol. 58, no. 4, pp. 1014–1019, Apr. 2010.

[10] J. Lee, H. Hong, and D. Yoon, "Stepped θ-QAM for high-order modulation," *Electron. Lett.*, vol. 53, no. 25, pp. 1676–1678, Dec. 2017.

[11] T. G. Markiewicz, "Construction and labeling of triangular QAM," *IEEE Commun. Lett.*, vol. 21, no. 8, pp. 1751–1754, Aug. 2017.

[12] M. Abramowitz and I. A. Stegun, *Handbook of Mathematical Functions: With Formulas, Graphs, and Mathematical Tables*, 9th ed. New York, NY, USA: Dover, 1970.

[13] J. Lee, D. Yoon, and K. Cho, "Error performance analysis of M-ary θ-QAM," *IEEE Trans. Veh. Technol.*, vol. 61, no. 3, pp. 1423–1427, Mar. 2012.

[14] J. Lassing, E. G. Strom, E. Agrell, and T. Ottosson, "Computation of the exact bit-error rate of coherent M-ary PSK with Gray code bit mapping," *IEEE Trans. Commun.*, vol. 51, no. 11, pp. 1758–1760, Nov. 2003.

[15] M. K. Simon and M.-S. Alouini, *Digital Communication over Fading Channels: A Unified Approach to Performance Analysis*, 2nd ed. Hoboken, NJ, USA: Wiley, 2005.

[16] J. Lee, D. Yoon, and S. K. Park, "Performance analysis of error probabilities for arbitrary 2-D signaling with I/Q unbalances over Nakagami-m fading channels," *IEICE Trans. Commun.*, vol. E91-B, no. 1, pp. 364–367, Jan. 2008.

SEONGJIN AHN received the B.S. degree in electronic engineering from Hanyang University, Seoul, Korea, in 2016, where he is currently pursuing the Ph.D. degree with the Department of Electronics and Computer Engineering. His research interests include digital communication theory and wireless communications.

DONGWEON YOON received the B.S. *(summa cum laude)*, M.S., and Ph.D. degrees in electronic communications engineering from Hanyang University, Seoul, Korea, in 1989, 1992, and 1995, respectively. From March 1995 to August 1997, he was an Assistant Professor with the Department of Electronic and Information Engineering, Dongseo University, Busan, Korea. From September 1997 to February 2004, he was an Associate Professor with the Department of Information and Communications Engineering, Daejeon University, Daejeon, Korea. Since March 2004, he has been with the Faculty of Hanyang University, Seoul, where he is currently a Professor with the Department of Electronic Engineering and the Director of the Signal Intelligence Research Center. His research interests include digital communications theory and system, detection and estimation, satellite and space communications, and wireless communications.